Changes of the Annual Precipitation over Central Asia in the Twenty-First Century Projected by Multimodels of CMIP5

ANNING HUANG, YANG ZHOU, YAOCUN ZHANG, AND DANQING HUANG

School of Atmospheric Sciences, Nanjing University, Nanjing, China

YONG ZHAO

Institute of Desert Meteorology, China Meteorology Administration, Urumqi, China

HAOMIN WU

School of Atmospheric Sciences, Nanjing University, Nanjing, and Lishui Meteorological Bureau, Lishui, China

(Manuscript received 18 January 2014, in final form 21 April 2014)

ABSTRACT

Based on the outputs of historical and future representative concentration pathway (RCP) experiments produced by 28 models from phase 5 of the Coupled Model Intercomparison Project (CMIP5), future changes in climatic mean, interannual standard deviation (ISD), and long-term trends of the annual precipitation over central Asia (CA) have been estimated. Under different emission scenarios during the twenty-first century, the climatic mean and ISD (long-term trends) of the annual precipitation over CA projected by the five best models' ensemble mean show very similar (quite different) spatial patterns to those in the twentieth century. Relatively stronger increasing rates (over 3 mm decade^{-1} in RCP2.6 and over 6 mm decade^{-1} in RCP4.5 and RCP8.5) are located over northern CA and the northeastern Tibetan Plateau. Compared to the situations in the twentieth century, the climatic mean, ISD, and long-term trends of the projected annual precipitation over most of CA under different emission scenarios exhibit robust increasing changes during the twenty-first century. The projected increasing changes in the climatic mean (ISD) of the CA annual mean range from 10% to 35% (10%–90%) under different emission scenarios with relatively large increases over Xinjiang, China (northern CA and Xinjiang). The increasing trends of the annual precipitation over most of CA are projected to intensify with relatively large increases (over 3–9 mm decade^{-1}) located over northern CA, the Tian Shan Mountains, and northern Tibet during the twenty-first century. In addition, the intensities of the increasing changes in the climatic mean, ISD, and trends of CA annual precipitation are intensified with the emissions increased correspondingly. Further analyses of the possible mechanisms related to the projected changes in precipitation indicate that the increases of the annual precipitation over CA in the twenty-first century are mainly attributed to the enhanced precipitable water that results from strengthened water vapor transport and surface evaporation.

1. Introduction

Global warming characterized by the global mean surface air temperature increase of 0.74° ± 0.18°C in the last 100 years (Solomon et al. 2007) has caused tremendous impacts on global and regional climate changes (Dai et al. 1998; Chen et al. 2010). In a warming world where the atmosphere can hold more water vapor, the hydrological cycle could become more active (Folland et al. 2001a). Recent and potential future increases in global temperatures are likely to affect the hydrologic cycle, including changes of precipitation and increases in extreme events (Sheffield and Wood 2008). Earlier studies show that the responses of regional precipitation changes to global warming differ regionally (Ma and Fu 2007) and the relationships between temperature increasing and precipitation variations differ in different regions (Hulme 1996). A wealth of previous studies indicate that arid and semiarid regions with scare

Corresponding author address: Dr. Yaocun Zhang, School of Atmospheric Sciences, Nanjing University, No. 22 Hankou Road, Nanjing, Jiangsu 210093, China.
E-mail: yczhang@nju.edu.cn

DOI: 10.1175/JCLI-D-14-00070.1

precipitation are prone to rapid hydrological, biological, and biogeochemical changes in response to global climatic change (Lioubimtseva et al. 1998) and have often been predicted to be among the most responsive ecosystems to higher carbon dioxide concentrations and global warming (Melillo et al. 1993; Smith et al. 2000).

As one of the largest arid and semiarid areas in the world, central Asia (CA) stretches from the Caspian Sea in the west to China in the east and from Afghanistan and Iran in the south to Russia in the north, covering the territory of five countries (Kazakhstan, Kyrgyzstan, Tajikistan, Turkmenistan, and Uzbekistan) and part of northwest China (Fig. 1) with an area of over $4 \times 10^6\,km^2$ and almost 60 million people. Located between the northern temperate zone and the southern subtropical zone, the westerlies-dominated CA (Lioubimtseva et al. 2005) is characterized by semiarid and arid climate conditions with a deficit of freshwater. The inhomogeneous climates over CA with great spatial variability are largely due to the heterogeneity associated with the complex terrain including high mountain ranges and flat low-level plains (Böhner 2006; Aizen et al. 1995; Narama et al. 2009) and are characterized by pronounced interannual precipitation variability (von Wehrden et al. 2010). Recent studies show that CA is one of the specific regions that are likely to be strongly affected by global warming (Solomon et al. 2007; Chen et al. 2010). During the last 100 years, the surface air temperature over CA exhibited a significant warming trend with an increasing rate of around $0.18°C\,decade^{-1}$, which is larger than the global average and twice the warming rate of the surface air temperature over the Northern Hemisphere (Chen et al. 2009). A recent study shows that the annual precipitation in CA is generally enhancing during the past 80 years with an apparent increasing trend in winter (Chen et al. 2011). This is quite different from the general characteristics of precipitation changes (Huang et al. 2012) over the subtropical land regions.

CA is a unique region among the world's ecosystems. Water is particularly scarce in CA, where the ecosystems largely depending on water provided by precipitation during the growing season are highly vulnerable and among the most responsive to global climatic change (Huxman and Smith 2001; Whitford 2002). The changes in climatic variables such as temperature and precipitation strongly affect the fragile ecosystems in CA (Lobell and Asner 2003; Lobell and Field 2007; Kucharik 2008; Deryng et al. 2011; Hsiang et al. 2011), which are especially highly sensitive to changes in the local hydrological cycle and characteristics of precipitation caused by global warming (Trenberth et al. 2003; Narisma et al. 2007). A recent study by Gessner et al. (2013) indicates that the vegetation development

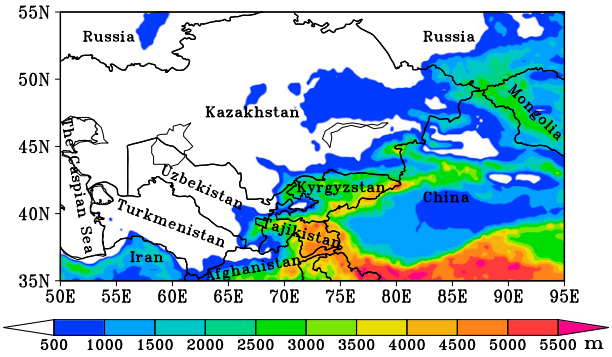

FIG. 1. Topography and administrative map of central Asia. Shadings show the topography height.

on nearly 80% of the CA land surface is sensitive to precipitation anomalies, particularly with a strong sensitivity of vegetation in areas with annual precipitation ranging from 100 to 400 mm.

Large hydrological year-to-year variations and associated implications for socioeconomics and ecology arise necessary studies on assessing long-term climate variations in the "climate change hot spot" of CA (Giorgi and Francisco 2000; Giorgi 2006) in view of projected climate changes (Viviroli et al. 2011; van Vuuren et al. 2011). A recent study shows that projections of precipitation amounts over CA are not fully consistent: The seasonal distribution of precipitation changes are projected with less precipitation in the central and southern parts of CA particularly during summer and an increase of winter precipitation in the northern and eastern parts (Lioubimtseva and Henebry 2009). These changes in climate have exacerbated water stress over CA (Siegfried et al. 2012).

Existing studies show that one of the most important social and political risks associated with climate change pertains to water availability (Dinar and Dinar 2003; Wolf et al. 2003). Understanding the variations of precipitation and the related water resources in the context of global warming is very important for the regional agriculture and economy in CA, which is one of the most vulnerable regions in the world to climate change. Uncertainties in the multiscale spatiotemporal variability of CA climate (Lioubimtseva et al. 2005) complicate the necessary assessment of regional climate characteristics and their future development under global warming.

Recently, phase 5 of the Coupled Model Intercomparison (CMIP5) of the Intergovernmental Panel on Climate Change (IPCC) Fifth Assessment Report (AR5) has provided the latest outputs from over 40 coupled general circulation models (CGCMs) developed by different institutes across the world (Taylor

et al. 2012). Based on these output data, most studies have focused on the future regional precipitation changes in response to global warming under different future emission scenarios (Bao 2012; Fyfe et al. 2012; Jiang and Tian 2013; Kharin et al. 2013; Knutti and Sedláček 2012; Wei and Bao 2012). However, much less attention has been paid to the future changes and detailed regional differences in the annual precipitation over CA in response to the global warming scenarios. To address these issues in detail, based on the latest results of the historical and different future emission scenario described as representative concentration pathway (RCP) experiments (Taylor et al. 2012) provided by the multiple CGCMs of CMIP5, such questions are concentrated in current study as follows: 1) How is the ability of each CMIP5 climate model in simulating the historical changes of the CA annual precipitation? 2) Can the ensemble mean derived from the outputs of models with good skills reproduce the characteristics of the CA annual precipitation? 3) What are the basic features of the future changes in the CA annual precipitation under different future emission scenarios in the twenty-first century with respect to the twentieth century based on the best models' ensemble mean? 4) What are the underlying possible mechanisms related to the changes in the annual precipitation over CA during the twenty-first century? Answering these questions is necessary and valuable for the policy makers to make policies and take actions for the challenges of the potential effects of climate changes over CA in the future.

The data and methodology are given in section 2. An evaluation of each model's performance in simulating the CA annual precipitation during the twentieth century is indicated in section 3. Spatial distributions of the projected changes in the annual precipitation over CA are shown in section 4. Possible underlying physical mechanisms are discussed in section 5. A summary of the results is provided in section 6.

2. Data and methodology

a. Data

The data used in this study are shown as follows:

1) The Climate Research Unit (CRU) time series version 3.10 (TS3.10; which supersedes CRU TS3.00) monthly dataset covering the global land with a horizontal resolution of 0.5° in longitude by 0.5° in latitude is provided by the University of East Anglia (Mitchell and Jones 2005). The CRU TS3.10 dataset is derived from the monthly observations at meteorological stations across the world's land areas during 1901–2009 (Harriset al. 2014). The dataset includes 10 variables (precipitation, cloud cover, diurnal temperature range, frost day frequency, potential evapotranspiration, daily mean temperature, daily minimum temperature, daily maximum temperature, vapor pressure, and wet day frequency). CRU TS3.10 data are produced by the same methodology as for the TS3.00 dataset. Slight differences which are not significant may be noticed between the results for a given time/location between the TS3.00 and TS3.10 versions because of additional data now being available. The new dataset compares with sparser observations very well. The different versions of CRU dataset have been widely used in studies of climate change (Houghton et al. 2001; Folland et al. 2001b; Jone et al. 2001; Brohan et al. 2006; Peterson and Manton 2008; Huang et al. 2012). In the current study, we only used the precipitation data from CRU TS3.10, which can be obtained online (at http://badc.nerc.ac.uk/data/cru/) to conduct model evaluation.
2) Monthly precipitation; surface heat fluxes; and atmospheric variables, including zonal (u) and meridional (v) components of wind speed, specific humidity, evaporation, and so on, at different pressure levels from the historical and RCP experiments of 28 CMIP5 coupled climate models (Table 1): The outputs from the historical (RCP2.6, RCP4.5, and RCP8.5) experiments cover the period of 1850–2005 (2006–2100). RCP2.6, RCP4.5, and RCP8.5 represent different future emission scenarios (van Vuuren et al. 2011) from low to high, respectively. For all models and experiments, the results of the first ensemble member (r1i1p1) are used in this study. All model outputs are interpolated onto the horizontal resolution of 0.5° × 0.5° using a bilinear interpolation method. More detailed information about the experimental designs of the historical and RCP experiments (Peters et al. 2013) can be found in Taylor et al. (2012).

b. Methodology

The analysis methods including the spatial correlation coefficient (SCC) that reveals the spatial distribution similarity between the model simulation and the observations; root-mean-square error (RMSE) that indicates the bias of the intensity between the simulation and observation; standard deviation (SD) that shows the variation or dispersion from the average; model spread (MS); and ratio of signal to noise (R_{SN}) are adopted in this study. The detailed descriptions for MS and R_{SN} are given in the following subsections:

TABLE 1. Information on the 28 CMIP5 climate models used in the current study.

Model No.	Model name	Model expansion	Institute, country	Horizontal resolution (lat × lon)
1	BCC_CSM1.1	Beijing Climate Center (BCC), Climate System Model, version 1.1	BCC, China Meteorological Administration, China	~2.8° × 2.8°
2	BCC_CSM1.1-m	BCC, Climate System Model, version 1.1m		~1.1° × 1.1°
3	BNU-ESM	Beijing Normal University (BNU)—Earth System Model	BNU, China	~2.8° × 2.8°
4	CanESM2	Second Generation Canadian Earth System Model	Canadian Centre for Climate Modelling and Analysis (CCCma), Canada	~2.8° × 2.8°
5	CCSM4	Community Climate System Model, version 4	National Center for Atmospheric Research (NCAR), United States	~1.25° × 1°
6	CESM1-CAM5	Community Earth System Model, version 1 (Community Atmosphere Model, version 5)	National Science Foundation, U.S. Department of Energy, and NCAR, United States	~1.25° × 1°
7	CNRM-CM5	Centre National de Recherches Météorologiques (CNRM) Coupled Global Climate Model, version 5	CNRM/Centre Europeen de Recherche et Formation Avancees en Calcul Scientifique, France	~1.4° × 1.4°
8	CSIRO Mk3.6.0	Commonwealth Scientific and Industrial Research Organisation (CSIRO) Mark 3.6.0	CSIRO in collaboration with the Queensland Climate Change Centre of Excellence, Australia	~1.87° × 1.85°
9	EC-EARTH	European Consortium (EC)-Earth Sytem Model	EC-EARTH Consortium	~1.1° × 1.1°
10	FGOALS-g2	Flexible Global Ocean–Atmosphere–Land System Model gridpoint, version 2.0	State Key Laboratory of Numerical Modeling for Atmospheric Sciences and Geophysical Fluid Dynamics (LASG), Institute of Atmospheric Physics, Chinese Academy of Sciences; and Center for Earth System Science (CESS), Tsinghua University, China	~2.8° × 2.8°
11	FIO-ESM	First Institute of Oceanography (FIO) Earth System Model	FIO, State Oceanographic Institute (SOA), China	~2.8° × 2.8°
12	GFDL CM3	Geophysical Fluid Dynamics Laboratory (GFDL) Climate Model, version 3	GFDL, United States	2.5° × 2°
13	GFDL-ESM2G	GFDL Earth System Model with Generalized Ocean Layer Dynamics (GOLD) component		~2.5° × 2°
14	GFDL-ESM2M	GFDL Earth System Model with Modular Ocean Model 4 (MOM4) component		~2.5° × 2°
15	GISS-E2-H	Goddard Institute for Space Studies (GISS) Model E2, coupled with the Hybrid Coordinate Ocean Model (HYCOM)	National Aeronautics and Space Administration (NASA) GISS, United States	2.5° × 2°
16	GISS-E2-R	GISS Model E2, coupled with the Russell ocean model		2.5° × 2°
17	HadGEM2-AO	Hadley Centre Global Environment Model, version 2—Atmosphere and Ocean	Met Office Hadley Centre, United Kingdom	1.875° × 1.25°
18	HadGEM2-ES	Hadley Centre Global Environment Model, version 2—Earth System		1.875° × 1.25°

TABLE 1. (*Continued*)

Model No.	Model name	Model expansion	Institute, country	Horizontal resolution (lat × lon)
19	IPSL-CM5A-LR	L'Institut Pierre-Simon Laplace Coupled Model (IPSL), version 5A, low resolution	IPSL, France	~3.75° × 1.9°
20	IPSL-CM5A-MR	IPSL, version 5A, mid resolution		~2.5° × 1.3°
21	MIROC5	Model for Interdisciplinary Research on Climate (MIROC), version 5	Japan Agency for Marine-Earth Science and Technology, Atmosphere and Ocean Research Institute (The University of Tokyo), and National Institute for Environmental Studies, Japan	~1.4° × 1.4°
22	MIROC-ESM	MIROC, Earth System Model		~2.8° × 2.8°
23	MIROC-ESM-CHEM	MIROC, Earth System Model, Chemistry Coupled		~2.8° × 2.8°
24	MPI-ESM-LR	Max Planck Institute Earth System Model, low resolution	Max Planck Institute for Meteorology (MPI-M), Germany	~1.87° × 1.85°
25	MPI-ESM-MR	Max Planck Institute Earth System Model, medium resolution		~1.87° × 1.85°
26	MRI-CGCM3	Meteorological Research Institute (MRI) Coupled Atmosphere–Ocean General Circulation Model, version 3	MRI, Japan	~1.1° × 1.1°
27	NorESM1-M	Norwegian Earth System Model, version 1 (intermediate resolution)	Norwegian Climate Centre, Norway	~2.5° × 1.9°
28	NorESM1-ME	Norwegian Earth System Model, version 1 (intermediate resolution with carbon cycle)		~2.5° × 1.9°

1) MODEL SPREAD

According to Huang et al. (2009), the MS is given by

$$\mathrm{MS} = \left[\frac{1}{n}\sum_{i=1}^{n}\left(\frac{x_i}{\overline{x}-1}\right)^2\right]^{1/2} \times 100\%, \qquad (1)$$

where n devotes the number of models; x_i is the simulation of the model number i; and $\overline{x}$ is the mean of the n models' results and can be calculated by $\overline{x} = 1/n\sum_{i=1}^{n} x_i$. The MS is a good index to measure the consistency of the results from multiple models. High (low) MS indicates low (high) consistency among the simulations from different models.

2) RATIO OF SIGNAL TO NOISE

The ratio of signal to noise of an N-yr average is defined according to Leith (1973) as

$$R_{\mathrm{SN}} = \frac{\Delta\overline{X}}{\sigma(X_2)}, \qquad (2)$$

where $\Delta\overline{X} = \overline{X}_2 - \overline{X}_1$ is the difference (change) between two climatic states X_1 and X_2 responding to different external forcings; $\overline{X}_1$ and $\overline{X}_2$ are the climatic means of X_1 and X_2 over N yr, respectively; $\sigma(X_2)$ is the standard deviation of X_2; and $R_{\mathrm{SN}} \geq 1$ indicates significant contribution of the forced climate change to the change in the finite-time mean climate.

In addition, in this study we adopt the standard least squares regression with linear slope and a two-tailed t test to examine all trends (Huang et al. 2012).

3. Model evaluation

The simulated precipitation of the historical experiment for the 28 CMIP5 models is compared with the CRU observed dataset to reveal each model's performance in simulating the annual precipitation over CA during 1901–2005.

To first reveal the MS of the simulated annual precipitation over CA among the 28 models, Fig. 2 gives the MS of the climatology, interannual SD (ISD), and long-term trends of the annual precipitation over CA during 1901–2005 simulated by the 28 CGCMs. Low MS (below 20%) of the climatology and ISD for the annual precipitation is located over most of CA, except for the Tarim basin of China (Figs. 2a,b), indicating that the annual precipitation climatology and ISD produced by

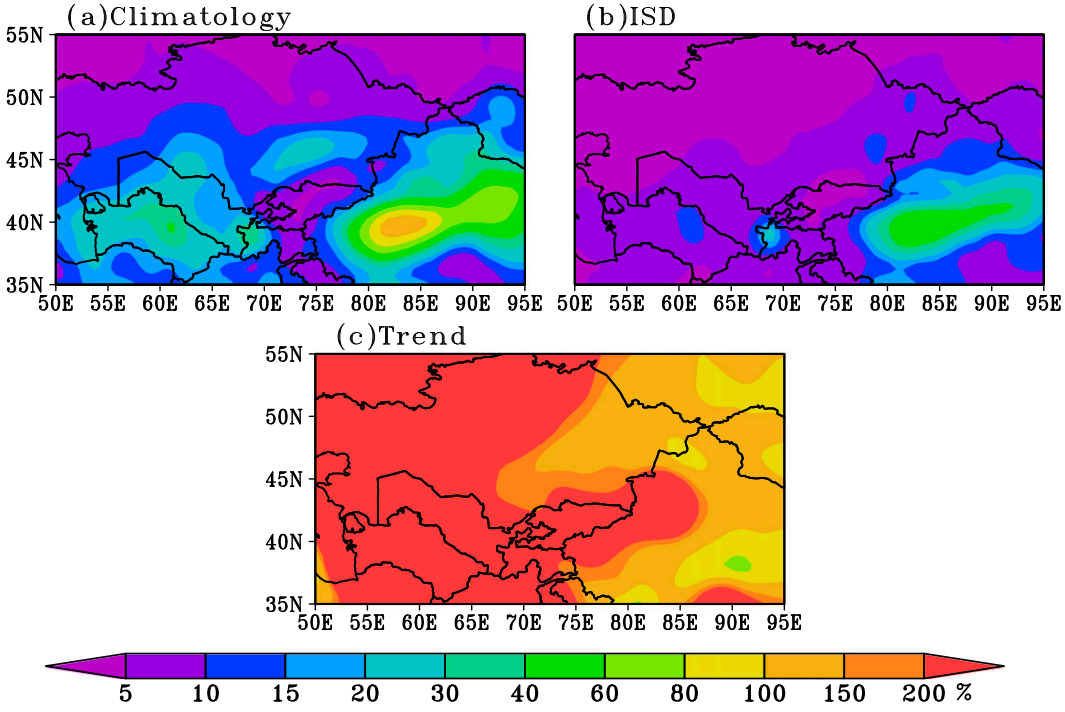

FIG. 2. The model spread of the (a) climatology, (b) ISD, and (c) long-term trends of the annual precipitation over CA simulated by the 28 models in the historical experiment during 1901–2005.

the 28 CGCMs show very high consistencies in most of CA, except that relatively large spread (over 40%) can be noted in the Tarim basin of China. However, the long-term trends of the annual precipitation over CA (Fig. 2c) produced by the 28 models show very large MS (over 100% in most of CA), suggesting that the 28 CMIP5 CGCMs have large inconsistencies in simulating the long-term trends of the CA annual precipitation. To objectively evaluate the performance of each model in simulating the annual precipitation, we score each model's ability in simulating the climatology, ISD, and long-term trends of the annual precipitation, which can explain much of the basic features inherent in climate variability.

Compared with the CRU data, we calculate the SCC, RMSE, and spatial standardized deviation ratios (which are derived from the spatial SD simulated by each model normalized by the observed spatial SD and reveal the similarity of the spatial heterogeneity between the simulation and observation; Seo and Ok 2013) for the climatology, ISD, and long-term trends of the CA annual precipitation in the historical experiment during 1901–2005. We score each model's performance in simulating the climatic mean, ISD, and long-term trend fields of the annual precipitation over CA with the following steps: 1) We rank the absolute differences between the spatial standardized deviation ratio and 1 and RMSEs (SCCs) for the 28 models from highest (lowest) to lowest (highest) with the sequence numbers ranging from 1 to 28. 2) Then we obtain the sequence number for each model in simulating a given aspect of the annual precipitation. 3) We score each model's ability in simulating the CA annual precipitation climatology, ISD, and long-term trends based on the sequence number: for example, for one model with the *i*th sequence number for SCC of the simulated and observed annual precipitation

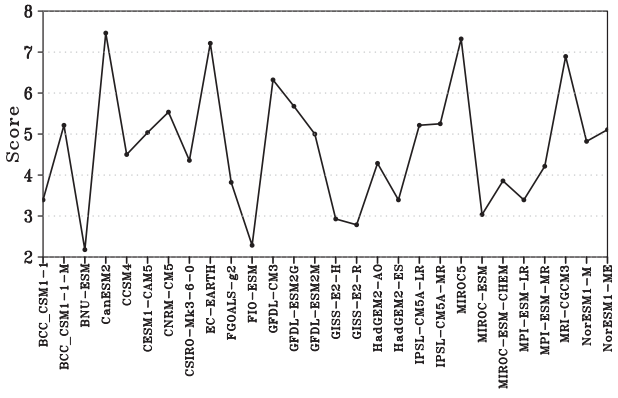

FIG. 3. Skill of each model in simulating the climatic mean, ISD, and long-term trends of the annual precipitation over CA during 1901–2005.

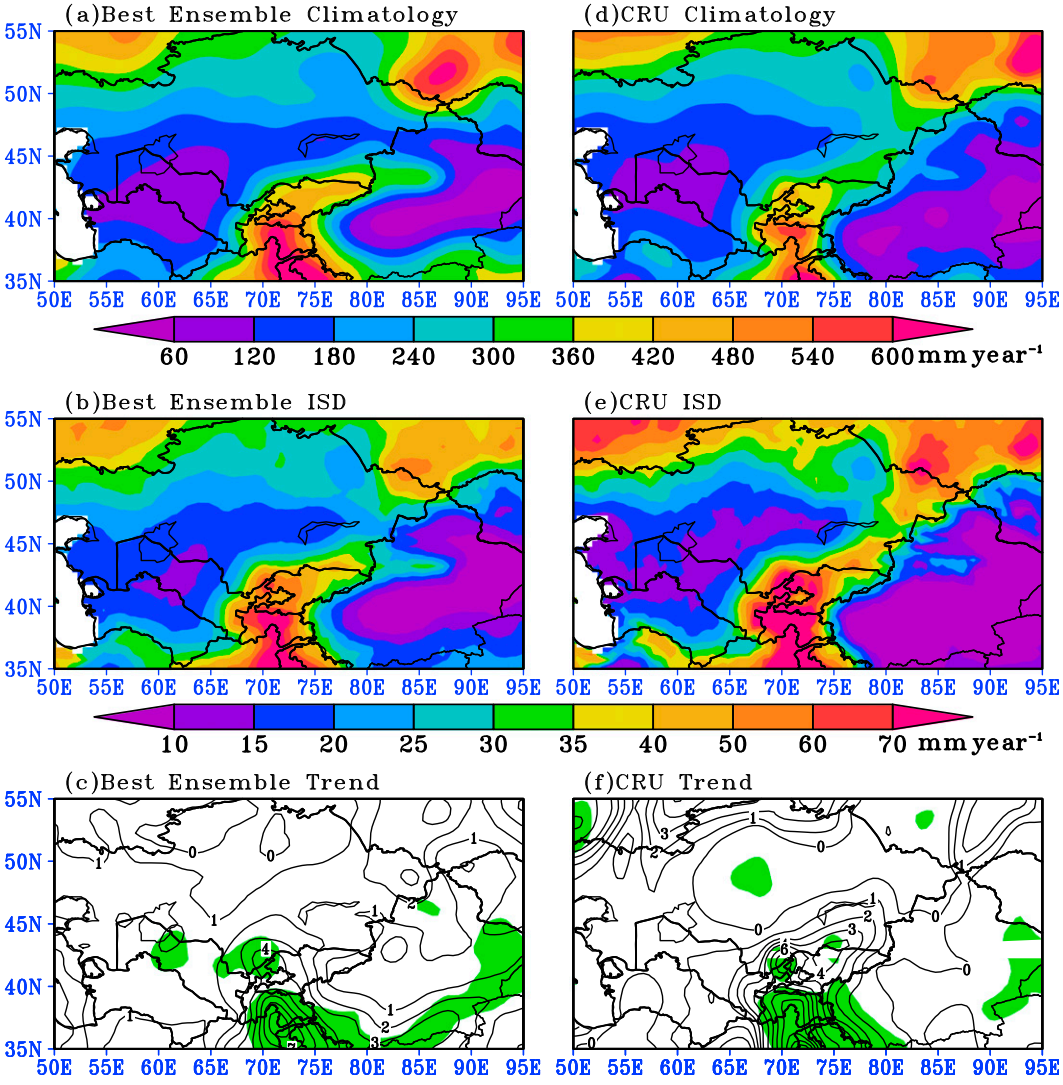

FIG. 4. The (a),(d) climatology, (b),(e) ISD, and (c),(f) long-term trends of the (left) five best models' ensemble mean and (right) CRU observed annual precipitation over CA during 1901–2005. In (c),(f), the contours indicate long-term trends (mm decade^{-1}) and areas over 95% significant confidence level of t test are shaded.

climatology, we can then score this model's performance in simulating the spatial pattern of the climatic mean field by $(i - 1)/(28 - 1)$ (where 28 is the total number of the models used in this study). It is obvious that the model with high sequence number show relative better ability in simulating a specified aspect. 4) Finally, we calculate the total value of the scores for each model in simulating the SCC, RMSE and spatial standardized deviation ratios of the modeled climatic mean, ISD, and long-term trends compared to the observations. So the total values of scores theoretically range from 0 to 9 and high (low) values indicate good (bad) performance. As shown in Fig. 3, the skills of the 28 models in simulating the climatic mean, ISD, and long-term trends of the annual precipitation over CA during 1901–2005 display large differences. Based on the skills shown in Fig. 3, we can pick out some models with good ability to conduct multimodel ensemble mean for the future projection of the annual precipitation over CA.

According to the skills of the 28 models shown in Fig. 3, five models (CanESM2, EC-EARTH, GFDL CM3, MIROC5, and MRI-CGCM3) with relatively better performance in simulating the annual precipitation over CA among the 28 models are picked out to do multimodel ensemble mean. The climatic mean, ISD, and long-term trends of the multimodel ensemble mean CA annual precipitation are calculated with the following

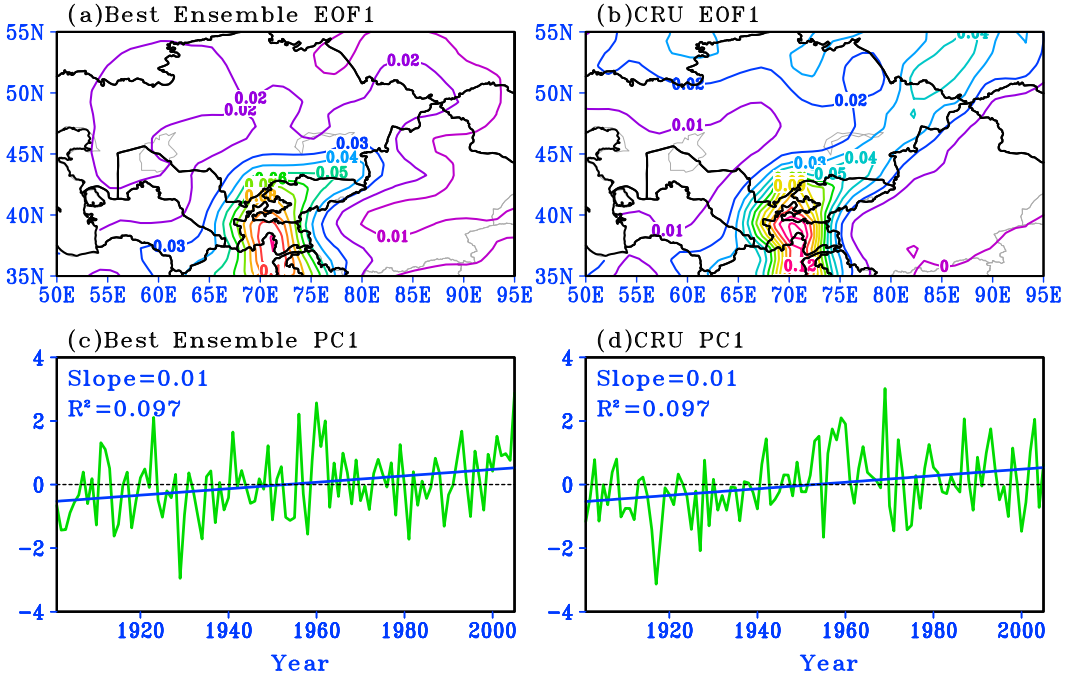

FIG. 5. The (a),(b) first leading EOF mode and (c),(d) corresponding normalized principal component indicated with green curves of the (left) five best models' ensemble mean and (right) CRU observed annual precipitation anomalies over CA during 1901–2005. In (c),(d) the blue lines show the long-term linear regression of the normalized principal components, the r^2 in the standard least squares regression indicates the square of correlation coefficients between two time series data, and the slope reveals the trend of PC1.

steps: 1) The yearly time series of the multimodel ensemble mean annual precipitation over CA is derived from the results of individual models over N yr. 2) Then the climatic mean, ISD, and trends are calculated based on the yearly time series dataset of N yr obtained in the first step.

To further illustrate the reliability of the five best models' ensemble mean, Fig. 4 gives the climatology, ISD, and long-term trends of the modeled and observed annual precipitation over CA during 1901–2005. As shown in Fig. 4d, the observed annual precipitation over large part of CA is less than 360 mm. However, the annual precipitation with the intensity less than 120 mm is located over most of Uzbekistan and south of Xinjiang, China. Meanwhile, three centers with relatively large annual precipitation with the intensity over 400 mm are located over the adjacent areas of southeastern Kyrgyzstan, northeastern Afghanistan, northern India, and northern Pakistan; southern Russia close to the northwestern border of the Kazakhstan; and southern Russia close to the adjacent regions of eastern Kazakhstan, northwestern China, and western Mongolia, respectively. It is obvious that the five best models' ensemble mean (Fig. 4a) well captured the intensity and spatial distributions of the observed annual precipitation climatology. Compared with the features in Fig. 4d, the ISD of the observed CA annual precipitation (Fig. 4e) shows a very similar distribution to the climatic mean fields. The five best models' ensemble mean also well produced the distribution of the observed ISD (Fig. 4b). As shown in Figs. 4c and 4f, both the five best models' ensemble mean and CRU annual precipitation exhibit slightly weak increasing trends over most of CA with significant increasing trends over 5 mm decade^{-1} located in the neighboring regions of Kyrgyzstan, eastern Afghanistan, northern India, and northern Pakistan during 1901–2005.

To give more detailed spatiotemporal distributions of the five best models' ensemble mean modeled and CRU observed annual precipitation anomalies during 1901–2005, empirical orthogonal function (EOF) analysis (North et al. 1982) is used in this study. Figures 5 and 6 give the two leading EOF modes (EOF1 and EOF2) of the annual precipitation over CA and their corresponding normalized principal component (PC) during 1901–2005.

As shown in Fig. 5b, the EOF1 mode of the observed annual precipitation anomalies over CA, which can explain the 22.4% of total variance, exhibits consistent

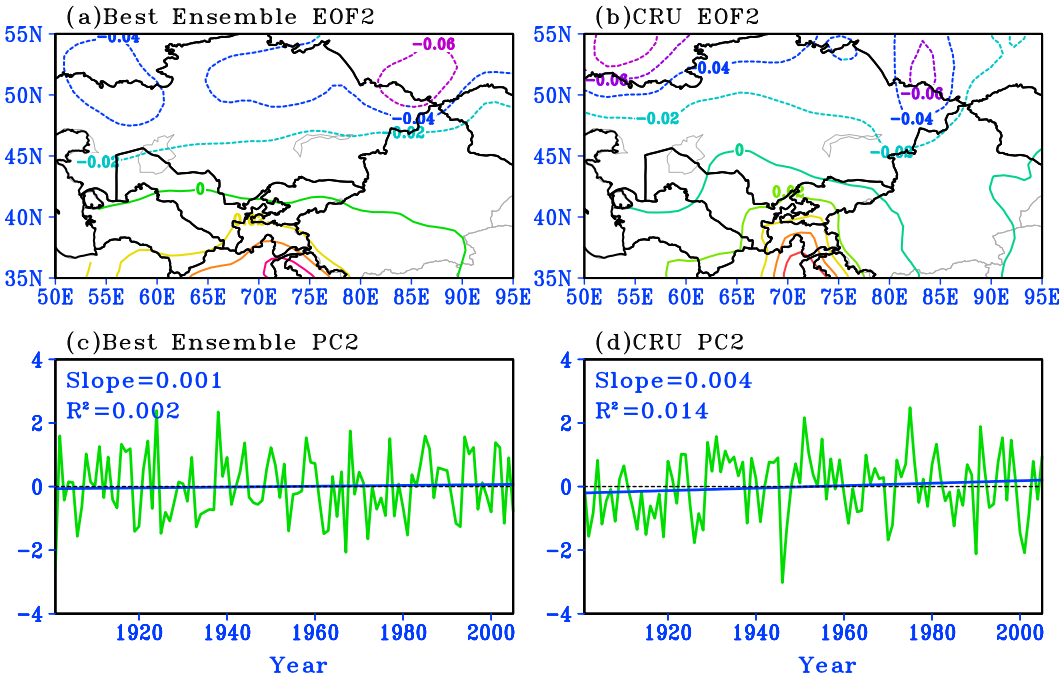

FIG. 6. As in Fig. 5, but for the EOF2 mode and corresponding normalized PC2.

changes over the entire region during 1901–2005 with the strongest (weakest) changing center located over northern Afghanistan and Tajikistan (Tarim basin of China). The PC1 for the observations (Fig. 5d) shows a significant increasing trend during 1901–2005. It is clearly shown in Figs. 5b and 5d that the observed annual precipitation over the whole CA is consistently dominated by an increasing trend. The EOF1 mode of the five best models' ensemble mean annual precipitation anomalies (Figs. 5a,c) shows comparable features to the observations. The EOF1 mode of the simulated annual precipitation anomalies can explain 22.7% of the total variance, which is close to that in the observations (22.4%).

However, the EOF2 mode and corresponding PC of the observed annual precipitation show reversed changes over northern and southern CA with no significant changing trend (Figs. 6b,d). Three relatively large changing centers are located over the adjacent areas of Kyrgyzstan, northeastern Afghanistan, northern India, and northern Pakistan; southern Russia close to the northwestern border of the Kazakhstan; and southern Russia close to the adjacent regions of eastern Kazakhstan, northwestern China, and western Mongolia, respectively. Compared with the observations, the five best models' ensemble mean also well reproduced the dominant features of the EOF2 mode of the annual precipitation anomalies over CA (Figs. 6a,c). The variance contribution rates of the EOF2 mode for simulation and observation are very comparable (15.4% versus 15%).

Overall, from the analyses mentioned above, the five best models' ensemble mean well reproduced the climatology, ISD, and long-term trends of the annual precipitation over CA and dominant spatiotemporal distributions of leading EOF modes of the precipitation anomalies. This enhances our confidence to some extent in the reliability of the projected annual precipitation over CA from the RCP experiments during the twenty-first century based on the five best models' ensemble mean.

4. Results of future projections

The climatic mean and ISD of the ensemble mean annual precipitation over CA projected by the five best models under different emission scenarios (Figs. 7a–f) during 2011–2100 obviously show very similar spatial patterns to those during 1901–2005 (Figs. 4a, b). However, the projected long-term trends of the annual precipitation shown in Figs. 7g–i display quite different distributions compared to the historical experiment simulation and the CRU data (Figs. 4c,f). The projected annual precipitation over most of CA consistently show increasing trends with stronger changing rates located over northern CA and the

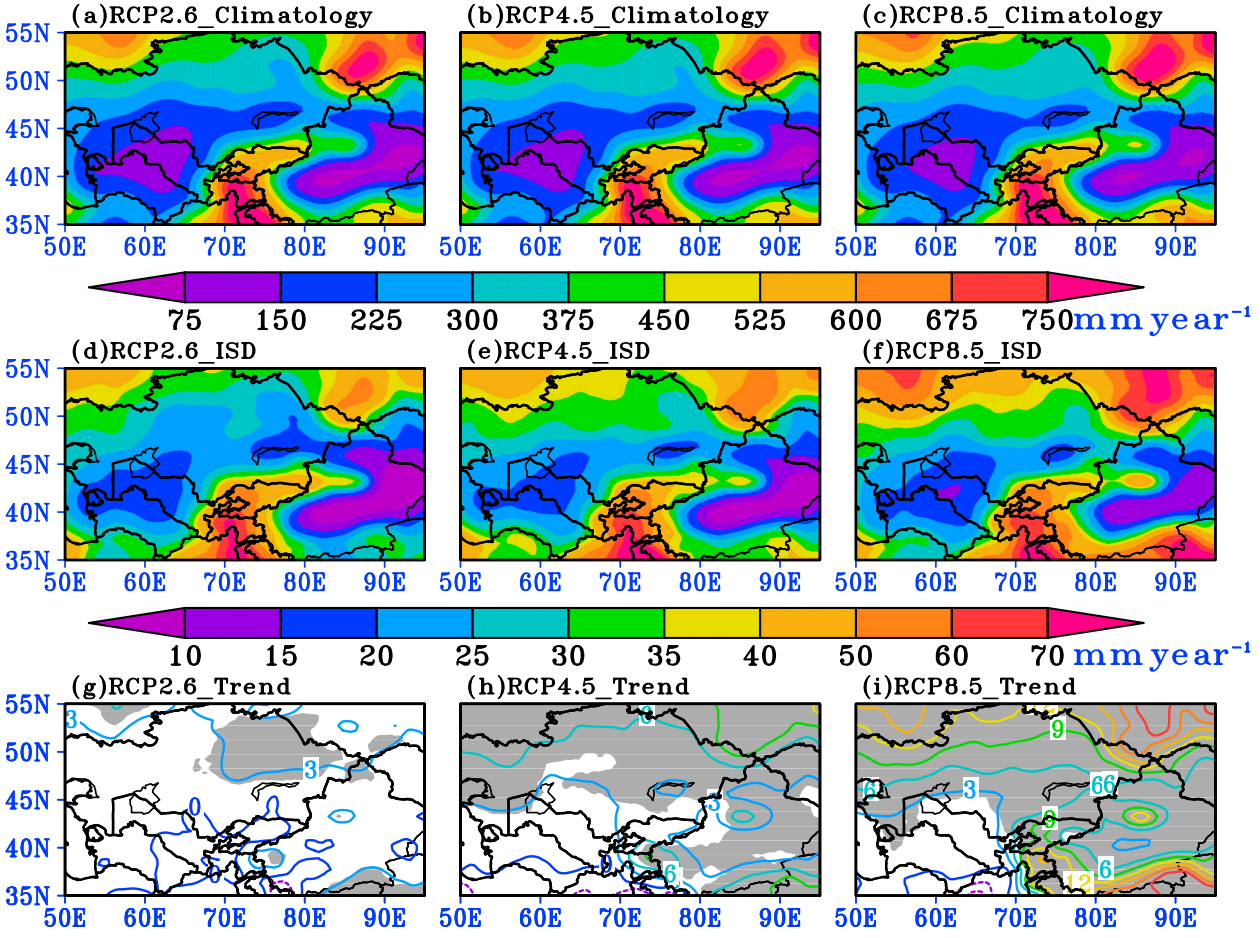

FIG. 7. The (a)–(c) climatic mean, (d)–(f) ISD, and (g)–(i) long-term trends of the five best models' ensemble mean annual precipitation over CA under different emission scenarios during 2011–2100. In (g)–(i), the contours indicate long-term trends of the annual precipitation over CA (mm decade^{-1}) and areas over 95% significant confidence level of t test are shaded.

northeastern Tibetan Plateau during 2011–2100, and the changing rates strengthen with the emissions increased.

To give more detailed spatiotemporal distributions of the CA annual precipitation, the EOF modes and corresponding PCs of the CA annual precipitation anomalies projected under different emission scenarios during 2011–2100 are given in Figs. 8 and 9. The EOF1 modes of the annual precipitation anomalies over CA under different emission scenarios (Figs. 8a–c) consistently show the same signs over the entire CA, indicating that the annual precipitation exhibits spatially consistent changes with the same signs during 2011–2100. As shown in Figs. 8d–f, the corresponding PC1 in the RCP2.6 experiment shows nonsignificant long-term trend; however, the results produced by RCP4.5 and RCP8.5 experiments show significant increasing trends, with slopes of 0.027 and 0.035 (r^2 of 0.483 and 0.840), respectively.

The EOF2 modes of the projected annual precipitation anomalies over CA (Figs. 9a–c) show opposite signs between northern and southern CA under different emission scenarios, suggesting that the annual precipitation over northern and southern CA displays inverse changes in the twenty-first century. Additionally, the RCP2.6 experiment (RCP4.5 and RCP8.5 experiments) produced a significant (nonsignificant) increasing trend of the PC2 (Figs. 9d–f). As a whole, the PC1 produced by the RCP4.5 and RCP8.5 experiments shows a significant increasing trend; however, the PC2 in the RCP2.6 experiment shows a significant increasing trend. Possible reasons related to such differences can be explained by the different experimental design of RCP2.6, in which the emission radiative forcing reaches a maximum near the middle of the twenty-first century before decreasing to an eventual nominal level of 2.6 W m^{-2}; however, in the RCP4.5 and RCP8.5 experiments the radiative forcing increases throughout the

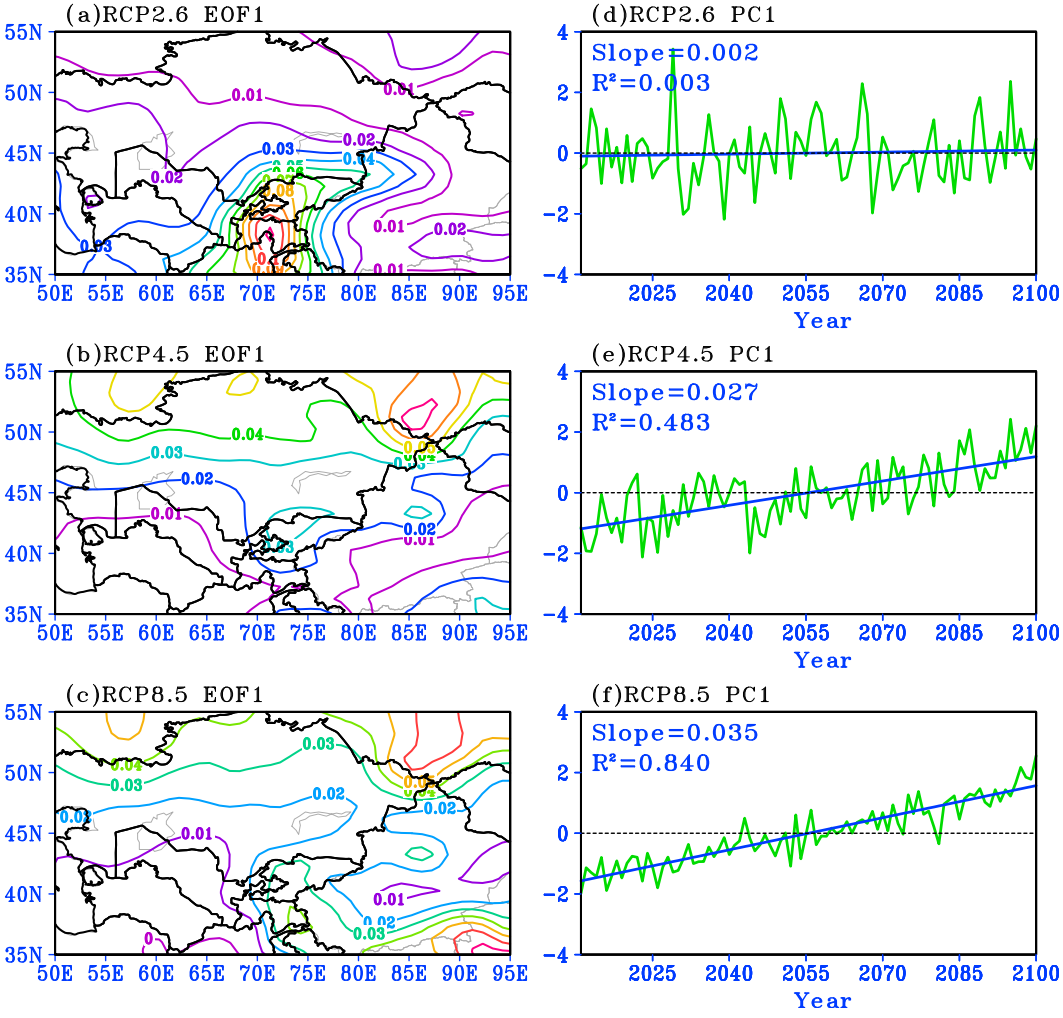

FIG. 8. The (a)–(c) EOF1 mode and (d)–(f) corresponding normalized PC1 indicated with green curves of the five best models' ensemble mean annual precipitation anomalies over CA under different emission scenarios during 2011–2100. In (d)–(f) the blue lines show the long-term linear regression of the normalized PC1, the r^2 in the standard least squares regression indicates the square of correlation coefficients between two time series data, and the slope reveals the trend of PC1.

twenty-first century (Taylor et al. 2012; van Vuuren et al. 2011). This explanation can be further confirmed by the EOF analysis of the annual precipitation anomalies during 2011–60, throughout which the emission radiative forcing in the RCP2.6, RCP4.5, and RCP8.5 experiments all increases (van Vuuren et al. 2011). The three experiments produced very similar spatial patterns for the leading two EOF modes of the annual precipitation anomalies during 2011–60 (not shown). The EOF1 modes and corresponding PC1s of the annual precipitation anomalies all consistently show increasing trends over the entire CA. However, the EOF2 modes and corresponding PC2s indicate that the annual precipitation over northern (southern) CA will increase (decrease) with nonsignificant trends. Comparisons of the results shown in Figs. 7g–i and Figs. 8 and 9 suggest that EOF1 (EOF2) mode of the projected annual precipitation anomalies over CA from RCP4.5 and RCP8.5 (RCP2.6) dominantly contribute to the changing trends of the CA annual precipitation during 2011–2100.

Figure 10 gives the fractional percentage changes of the climatic mean and ISD of the annual precipitation over CA and the changes in long-term trends from different RCP experiments during 2011–2100 relative to the results of the historical experiment during 1911–2000. The fractional percentage changes in the climatic mean fields under different emission scenarios during 2011–2100 (Figs. 10a–c) all exhibit significant increases in the annual precipitation over almost the entire CA by 10%–35% with a maximal increasing center located

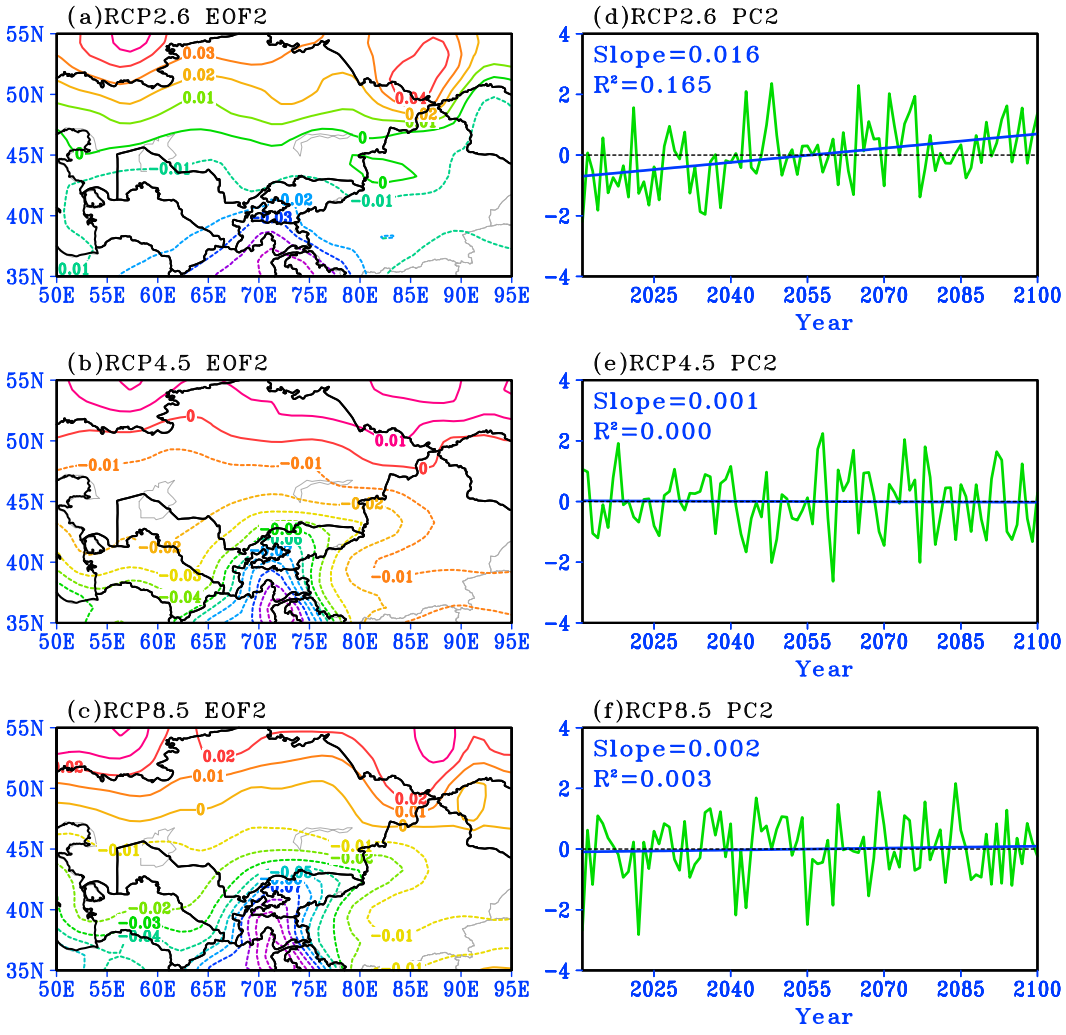

FIG. 9. As in Fig. 8, but for the EOF2 mode and corresponding normalized PC2.

over the Tarim basin of China. Meanwhile, with the emissions enhanced, the fractional percentage changes of the CA annual precipitation increase correspondingly. Changes in the ISD under different emission scenarios during 2011–2100 (Figs. 10d–f) are also significantly increased by 15%–90% with relative large changes located over northern and eastern CA, indicating that the variations of the CA annual precipitation will become more unstable in the twenty-first century under a warming climate. Furthermore, the increasing changes in the ISD will intensify with emissions increased.

The changes in the long-term trends of the projected annual precipitation under different emission scenarios during 2011–2100 (Figs. 10g–i) are increased over most of CA relative to 1911–2000 with the trends ranging from 0 to 12 mm decade^{-1}, signifying that the annual precipitation over most of CA is projected to increase at faster rates under different RCPs in the twenty-first century. Relatively large increasing changes can be found over northern CA, the Tian Shan Mountains, and northern Tibet and the increasing intensity strengthens under the emission scenarios from low to high. The annual precipitation over north Afghanistan and part of Tajikistan during 2011–2100 exhibit decreasing changes in the long-term trends compared to those in the twentieth century and the decreasing changes will weaken with the emissions increased. The regions with decreasing changes in the long-term trends of the annual precipitation contract from a relatively larger extent in RCP2.6 to small extent in RCP8.5. Overall, under the emission scenarios from low to high, the increasing trends of the annual precipitation over most of CA are projected to intensify in the twenty-first century. This is consistent with the results shown in Figs. 7g–i.

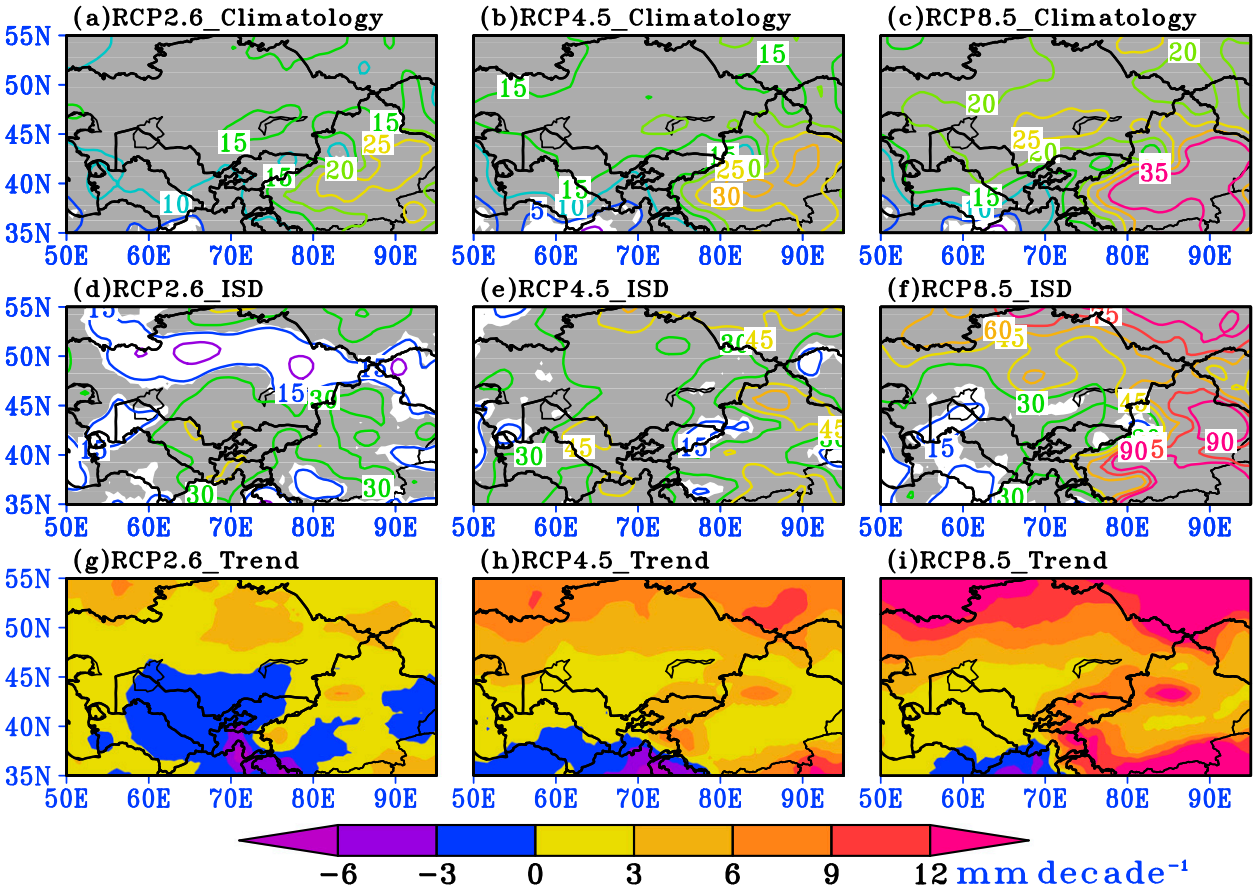

FIG. 10. Fractional percentage changes (%; contours) in the (a)–(c) climatic mean and (d)–(f) ISD of the CA annual precipitation projected by the five best models' ensemble mean under different emission scenarios during 2011–2100 with respect to 1911–2000. The regions over 95% significant confidence level of *t* test in (a)–(c) and *f* test in (d)–(f) are shaded. (g)–(i) Shadings show the changes in the long–term trends of the five best models' ensemble mean annual precipitation over CA under different emission scenarios during 2011–2100 relative to 1911–2000.

To further illustrate whether the five best models are consistent in projecting the future precipitation changes or not, we calculated the MS of the factional percentage changes in the climatic mean, ISD of the CA annual precipitation, and changes in the long-term trends produced by the five best individual models (not shown) in 2011–2100 under different RCPs with respect to the historical simulations in 1911–2000. Small MS values (below 20%) of the fractional percentage changes of climatic mean fields are located over most of CA, except southwestern CA and the central Tian Shan Mountains, where the MS values are relatively larger (over 30%). The changes in the long-term trends of the CA annual precipitation produced by the five best individual models show relatively small (large) MS over northern and southeastern CA (southwestern CA), with the values below 30% (over 60%). The MS of the ISD shows complex distributions compared with climatic mean and trend fields: The values range from 5% to 120% with relatively large values located over CA under RCP2.6 and RCP4.5. Overall, the MS decreases under the emission scenarios from low to high, suggesting that the uncertainties and inconsistency of the projected CA annual precipitation changes among the five best individual models reduces with the emissions increased. Under RCP8.5, the five best models produce much higher consistent changes in the CA annual precipitation. However, under RCP2.6, the projected changes in the ISD and trends, especially the trends, show a much larger inconsistency. Despite these uncertainties in the changes projected by the five best individual models under different RCPs, the uncertainties can be reduced through the multimodel ensemble (Huang et al. 2013).

To see if the changes in the climatic mean, ISD, and long-term trends of the CA annual precipitation during 2011–2100 shown in Fig. 10 are robust or not, Fig. 11 gives the changes in the annual precipitation over CA

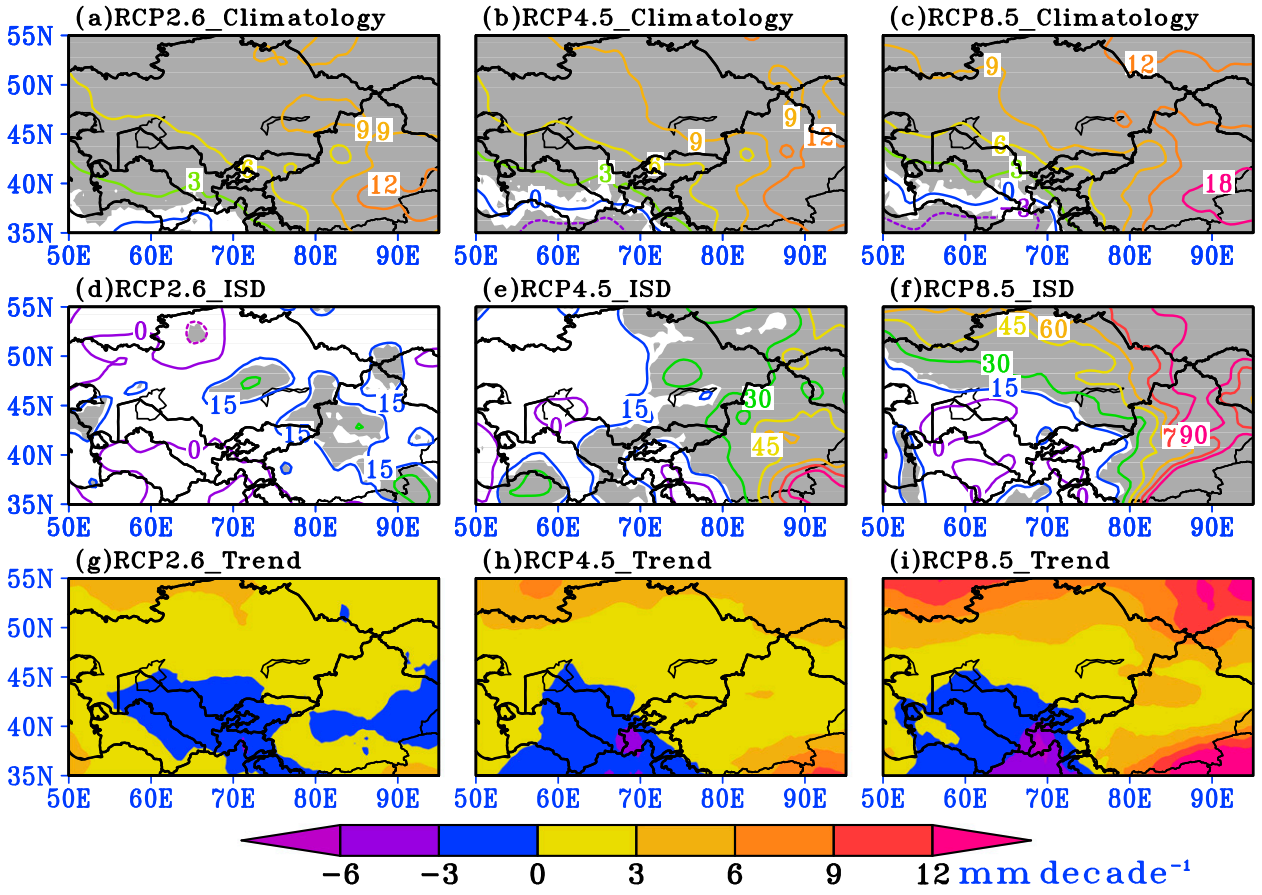

FIG. 11. As in Fig. 10, but for the 28 models' ensemble mean.

under different future emission scenarios relative to the situations of 1911–2000 based on the 28 models' ensemble mean. Compared with the features shown in Fig. 10, despite some differences in the intensities of the changes in the climatic mean, ISD, and long-term trends of the CA annual precipitation between the 28 models' ensemble mean and the five best models' ensemble, the spatial patterns are very comparable. In addition, the projected changes in the climatology, ISD, and long-term trends of the annual precipitation produced by the 28 models' ensemble and the five best models' ensemble over most of CA all consistently show strengthened intensities with the emissions enhanced. Further analysis shows that the signal-to-noise ratios of the changes in the CA annual precipitation based on the five best models' ensemble mean (not shown) over most of CA are greater than 1.0 under different RCPs, indicating that the changes in the annual precipitation over most of CA are significantly affected by the external forcing and further confirming the robust significance of the results shown in Fig. 10.

Overall, comparisons of Figs. 11 and 10 further confirm that the climatic mean, ISD, and long-term trends of the annual precipitation over most of CA projected in different RCPs exhibit robust increasing changes during the twenty-first century compared to the twentieth century. Furthermore, the intensities of the increasing changes are intensified with the emissions increased.

5. Possible mechanisms

The possible mechanisms related to the changes in the annual precipitation over CA projected under different emission scenarios will be revealed in this section. Figure 12 first gives the projected changes in the annual mean precipitation, vertically integrated water vapor transport flux, and atmospheric column water vapor content (precipitable water) over CA during 2011–2100 relative to 1911–2000. From Figs. 12a–c, the anomalous southwest water vapor transport flux prevails over CA under different emission scenarios, suggesting that the future water vapor transport flux from low latitudes under different RCPs will be strengthened. The projected precipitable water (Figs. 12d–f) under different emission scenarios is increased by 16%–40%, with the

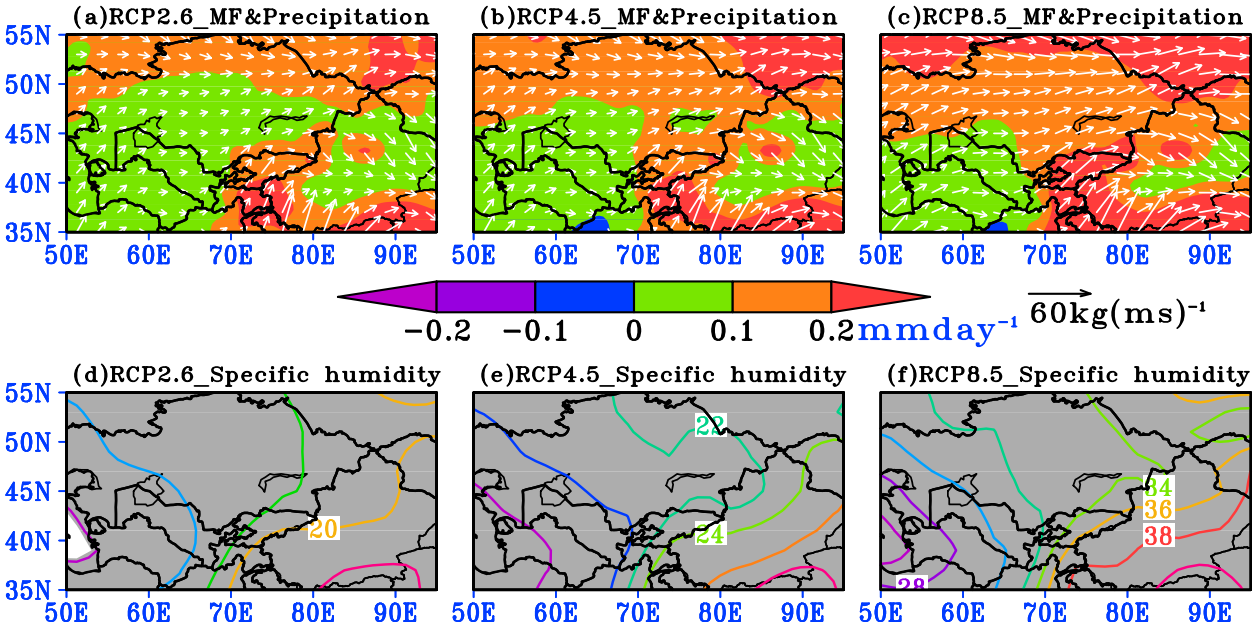

FIG. 12. (a)–(c) Changes in the annual mean precipitation (shaded) and vertically integrated (surface–300 hPa) water vapor transport flux (vector) over CA projected by the five best models' ensemble mean under different emission scenarios during 2011–2100 with respect to 1911–2000. (d)–(f) Fractional percentage changes (%; contours) in the annual mean vertically integrated (surface–300 hPa) specific humidity over CA during 2011–2100 relative to 1911–2000. The regions over the 95% significant confidence level of *t* test in (d)–(f) are shaded.

largest changing center located over southeastern CA. In addition, with the emissions increased the anomalous southwest water vapor flux, precipitation, and precipitable water are enhanced accordingly. These features of the changes in the water vapor transport and the precipitable water during 2011–2100 correspond well with the changes in precipitation shown in Figs. 10a–c. It is obvious that the increased precipitation over CA resulted from the strengthened water vapor transport and the enhanced precipitable water.

To further indicate the import processes associated with the changes in the annual precipitation over CA, we estimate each component of the moisture budget equation (Hsu et al. 2012) based on the formula

$$E + \left[-\frac{1}{g}\int_{300}^{p_s} \mathbf{V}\cdot(q\mathbf{V})\,dp\right] - P - \mathrm{Res} = 0, \qquad (3)$$

where E is evaporation from the surface, P is precipitation, q is specific humidity, $\mathbf{V}$ is the horizontal wind vector, g is the acceleration of gravity, and p is pressure. The second term of Eq. (3) represents the moisture flux convergence (MFC) vertically integrated from the surface to 300 hPa. Because the calculation is based on the monthly data, the residual (Res) is associated with the moisture tendency, contributions from the submonthly processes, computational errors, and so on. The MFC term in Eq. (3) can be subdivided into two terms: contributions from horizontal moisture advection (MD) $-\mathbf{V}\cdot\nabla q$ and moisture divergence associated with mass convergence (MC) $-q\nabla\cdot\mathbf{V}$.

Figure 13 gives the differences in the annual mean surface evaporation, MFC, and precipitation between the twenty-first century and the twentieth century. As shown in Figs. 13a–c, compared to the period of 1911–2000, the projected surface evaporation during 2011–2100 under different emission scenarios displays a prominent increase over the entire CA. Relatively large increased evaporation produced by RCP4.5 and RCP8.5 with the intensity over 0.15 mm day^{-1} is located over northern CA, the Caspian Sea, the Tian Shan Mountains, and mountain areas of southeastern CA. In addition, with the emissions increased the projected increases in the evaporation intensify correspondingly. From Figs. 13d–f, the projected MFC show both increasing and decreasing changes over CA. Meanwhile, different RCP experiments produced similar spatial distributions of the changes in MFC. Relatively large increased MFC can be found over northern CA and the southwestern part of the Tarim basin of China, with the intensity over 0.45 mm day^{-1}. Relatively large decreased MFC with the intensity over 0.3 mm day^{-1} is located over the adjacent areas of Turkmenistan, Uzbekistan, Afghanistan, and Tajikistan and the adjacent

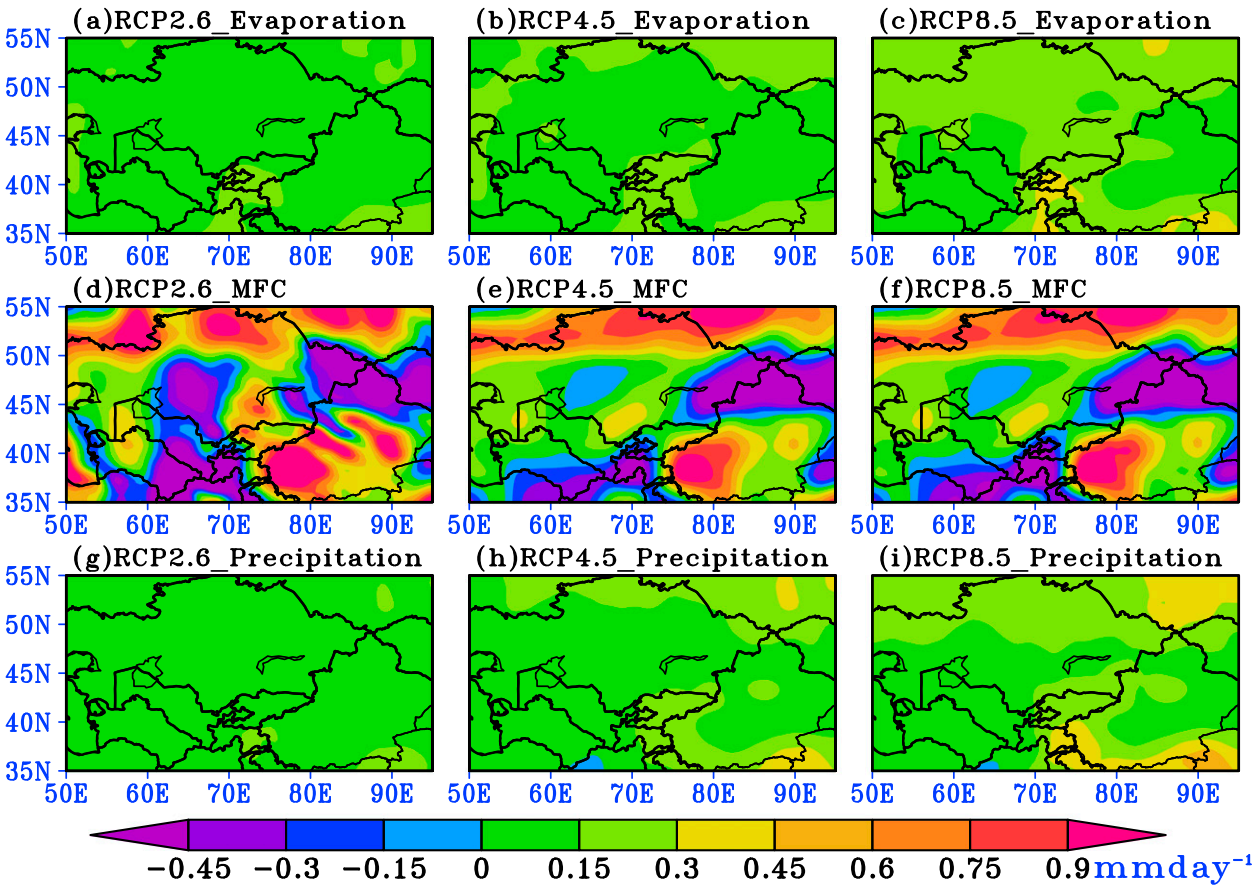

FIG. 13. Changes in the (a)–(c) annual mean surface evaporation, (d)–(f) vertically integrated (surface–300 hPa) moist flux convergence, and (g)–(i) precipitation over CA projected by the five best models' ensemble mean under different emission scenarios during 2011–2100 with respect to 1911–2000.

areas of Kazakhstan, Russia, Mongolia, and China. Comparisons of Figs. 13a–c and 13g–i show that the spatial patterns of the future changes in precipitation and evaporation exhibit very similar features, suggesting that the strengthening precipitation over CA leads to the increasing evaporation over CA, which is dominated by inland arid climate.

To reveal the relative contributions of the changes in MC and MD to MFC, Fig. 14 further gives the changes of MC and MD projected by different RCPs during 2011–2100 relative to 1911–2000. Overall, the projected changes of MD are largely weaker than those of MC. Compared with the features of the changes in the MFC shown in Figs. 13d–f, it is clear that the changes of MFC mainly resulted from those of MC.

To clearly illustrate the contribution of each component of the moisture budget in Eq. (3), Fig. 15 shows the regionally averaged future changes in the annual mean MC, MD, evaporation, precipitation, and Res over CA projected by different RCP experiments during 2011–2100 with respect to 1911–2000. The five components of the moisture budget are projected to increase in the twenty-first century. The future changes in the domain-averaged MC and Res over CA under different emission scenarios are the greatest among the five terms. The MC shows larger increases than MD, suggesting that the future increases in MFC mainly resulted from those of MC; this is consistent with the features shown in Figs. 13d–f and 14. The projected future changes in the precipitation, evaporation, and MD will be intensified with the emissions increased. However, the future changes in the MC and Res will be reduced under the emission scenarios from low to high. The precipitation and evaporation over CA show very comparable changes; further confirming that the intensified precipitation, which resulted from the enhanced precipitable water and strengthened water vapor transport, leads to the increased evaporation over CA, as shown in Figs. 12 and 13.

The differences between precipitation and evaporation (DPE) can well represent the net freshwater gain by the surface (Walsh et al. 1998). To further indicate the future changes in the annual mean DPE over CA, Fig. 16

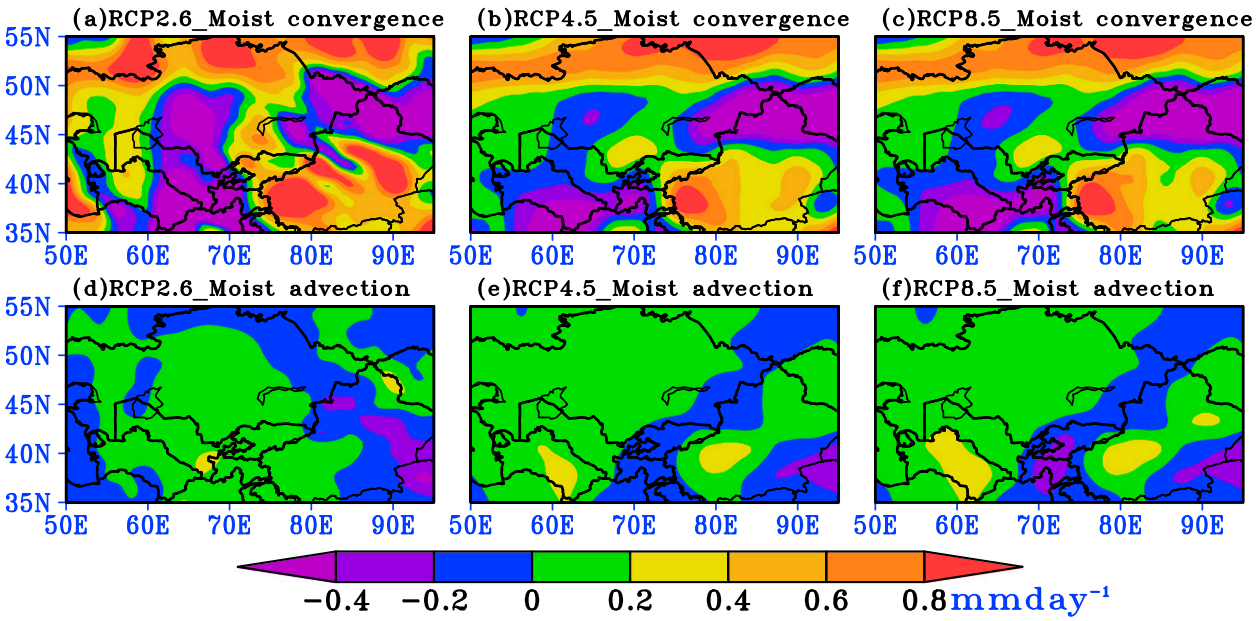

FIG. 14. Changes in the annual mean vertically integrated (surface–300 hPa) (a)–(c) moist convergence and (d)–(f) moist advection over CA projected by the five best models' ensemble mean under different emission scenarios during 2011–2100 relative to 1911–2000.

exhibits the projected changes in the annual mean DPE over CA under different emission scenarios during 2011–2100 compared to 1911–2000. It is clear that the projected changes in the annual mean DPE under different emission scenarios display a very similar spatial pattern. The annual mean DPE in 2011–2100 decreases (increases) over western (eastern) CA, indicating reduced (intensified) net freshwater gain by the surface over western (eastern) CA in the future. With the emissions increased, the regions occupied by the decreased (increased) DPE will enlarge (shrink) in the twenty-first century.

6. Concluding remarks

In this study, future changes in the annual precipitation over CA during 2011–2100 have been estimated based on the outputs of the historical and RCP experiments (RCP2.6, RCP4.5, and RCP8.5) with the emission scenarios from low to high produced by the 28 CMIP5 models of IPCC AR5. Comparing the historical experiment simulations from the 28 CMIP5 models with the observations, we first examined each model's performance in simulating the climatic mean, ISD, and long-term trends of the annual precipitation over CA during 1901–2005. Based on the skill of each model, five models (CanESM2, EC-EARTH, GFDL CM3, MIROC5, and MRI-CGCM3) with good ability are picked out to conduct a multimodel ensemble mean. Comparisons of the historical experiment simulation of the five best models' ensemble mean with the CRU observation show that climatic mean, ISD, long-term trends, and dominant spatiotemporal distributions of the annual precipitation over CA during 1901–2005 are well simulated. The climatic mean and ISD (long-term trends) of the annual precipitation over CA projected by the five best models' ensemble mean under different emission scenarios during 2011–2100 obviously show very similar (quite different) spatial distribution patterns to those in the twentieth century. The annual precipitation over most of CA under different emission scenarios consistently shows increasing trends during 2011–2100 with relatively large increasing rates (over 3 mm decade^{-1} in RCP2.6 and over 6 mm decade^{-1} in RCP4.5 and RCP8.5) located over northern CA and the northeastern Tibetan Plateau. Additionally, with the emissions increased the increasing rates of the annual precipitation over CA intensify correspondingly. Compared with the situations in the twentieth century, the fractional percentage changes in the climatic mean and ISD of the annual precipitation over CA under different RCPs are projected to significantly increase in the twenty-first century. Large increases in the climatic mean (ISD) fields are located over the Xinjiang province of China (northern CA and Xinjiang). The projected changes in long-term trends under different emission scenarios show that the CA annual precipitation will increase at faster rates in the twenty-first century with respect to the twentieth century. Overall, the intensities of the increasing changes in the climatic

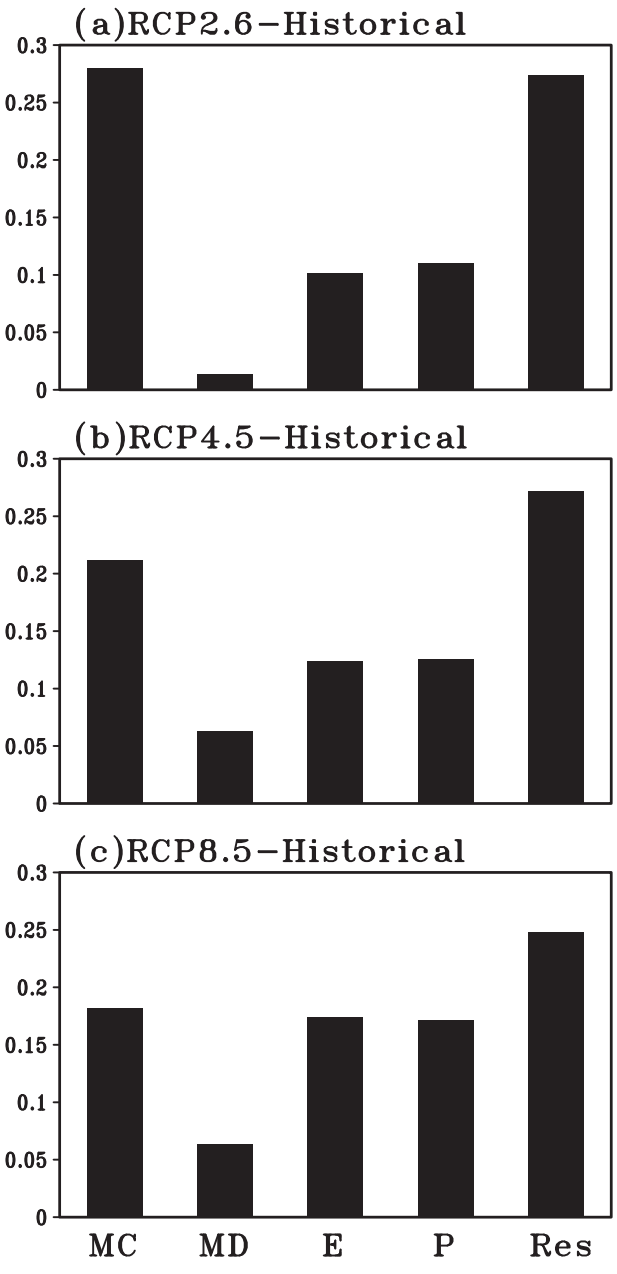

FIG. 15. Changes in each component of the moisture budget regionally averaged over CA (50°–95°E, 35°–55°N) projected by the five best models' ensemble mean under different emission scenarios during 2011–2100 relative to 1911–2000 (mm day^{-1}).

mean, ISD, and long-term trends of the CA annual precipitation are enhanced with the emissions increased. In addition, the spatial distributions of the long-term trends of the projected annual precipitation over CA from RCP2.6 (RCP4.5 and RCP8.5) are dominated by the EOF2 (EOF1) modes. Further comparisons of the 28 models' ensemble mean and the five best models' ensemble mean and analysis of the signal-to-noise ratios confirm that the climatic mean, ISD, and long-term trends of the projected annual precipitation over most of CA under different emission scenarios exhibit robust significant increasing changes during twenty-first century relative to the twentieth century. Possible mechanisms suggest that the projected increases of the annual precipitation over CA in the twenty-first century are mainly attributed to the increased precipitable water resulted from the strengthened water vapor transport and surface evaporation. Compared to the twentieth century, the changes in the annual mean DPE during 2011–2100 indicate reduced (intensified) net freshwater gain by the surface over western (eastern) CA in the future. Furthermore, the regions occupied by the decreased (increased) DPE will enlarge (shrink) with the emissions increased during 2011–2100.

In this study, we concentrated on the characteristics of the projected changes in the annual precipitation over CA and related possible underlying mechanisms during the twenty-first century. Primary analysis of the changes in climatic mean and long-term trends of the domain-averaged CA precipitation during 2011–2100 relative to 1911–2000 (not shown) suggests that relatively large (small) changes in the climatic mean and long-term trends of the CA precipitation occur in winter and spring (summer and autumn); this is consistent with the findings of Lioubimtseva and Henebry (2009). The projected changes of the CA precipitation under the three emission scenarios in spring are the greatest compared to the other seasons. However, the smallest changes among the four seasons are projected to occur in autumn (summer) under RCP2.6 and RCP4.5 (RCP8.5). Overall, the changes in both climatic mean and long-term trends of the annual precipitation over CA are largely resulted from those in winter and spring. Considering the limitation in the length of the current manuscript, more comprehensive analyses of the changes in the CA precipitation at different seasons cannot be completely included. To reveal the in-depth changes in the precipitation for different seasons, especially the crop growth season, and their contributions to annual changes is necessary and valuable for future work.

Acknowledgments. This research was supported by the Cooperation Program of National International Technological (2010DFA92720-14), National Natural Science Foundation of China under Grant 41175086, National Basic Research Program of China (973 Program) under Grant 2010CB951001, and the Jiangsu Collaborative Innovation Center for Climate Change. We acknowledge the World Climate Research Programme's Working Group on Coupled Modeling, which is responsible for CMIP, and we thank the climate

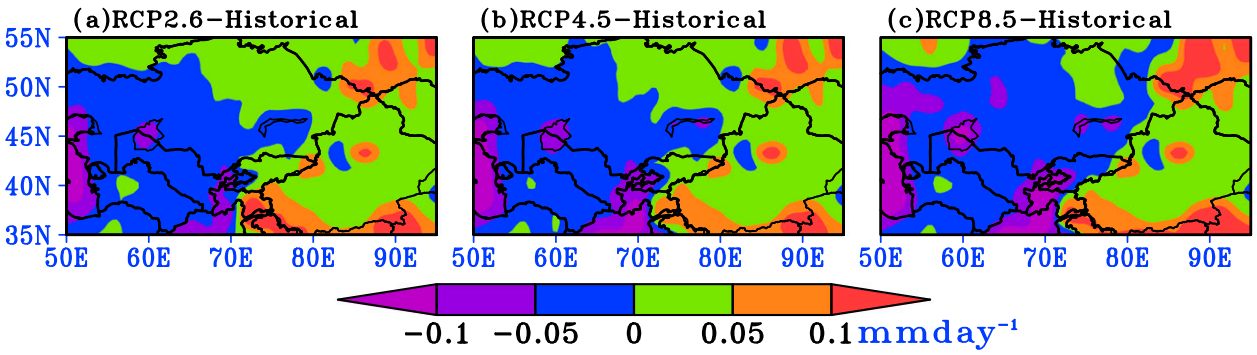

FIG. 16. Changes in the annual mean differences between precipitation and evaporation over CA projected by the five best models' ensemble mean under different emission scenarios during 2011–2100 with respect to 1911–2000.

modeling groups for making their model output available. We also thank the University of East Anglia for making and releasing the CRU TS3.10 dataset. We are grateful to three anonymous reviewers and editor Renguang Wu for their very thoughtful and constructive suggestions.

REFERENCES

Aizen, V. B., E. M. Aizen, and J. M. Melack, 1995: Climate, snow cover, glaciers, and runoff in the Tien Shan, central Asia. *J. Amer. Water Resour. Assoc.,* **31,** 1113–1129, doi:10.1111/j.1752-1688.1995.tb03426.x.

Bao, Q., 2012: Projected changes in Asian summer monsoons in RCP scenarios of CMIP5. *Atmos. Oceanic Sci. Lett.,* **5,** 43–48.

Böhner, J., 2006: General climatic controls and topoclimatic variations in Central and High Asia. *Boreas,* **35,** 279–295, doi:10.1111/j.1502-3885.2006.tb01158.x.

Brohan, P., J. Kennedy, I. Harris, S. F. B. Tett, and P. D. Jones, 2006: Uncertainty estimates in regional and global observed temperature changes: A new dataset from 1850. *J. Geophys. Res.,* **111,** D12106, doi:10.1029/2005JD006548.

Chen, F., J. Wang, L. Jin, Q. Zhang, J. Li, and J. Chen, 2009: Rapid warming in mid-latitude central Asia for the past 100 years. *Front. Earth Sci. China,* **3,** 42–50, doi:10.1007/s11707-009-0013-9.

——, and Coauthors, 2010: Moisture changes over the last millennium in arid central Asia: A review, synthesis and comparison with monsoon region. *Quat. Sci. Rev.,* **29,** 1055–1068, doi:10.1016/j.quascirev.2010.01.005.

——, W. Huang, L. Jin, J. Chen, and J. Wang, 2011: Spatiotemporal precipitation variations in the arid central Asia in the context of global warming. *Sci. China Earth Sci.,* **54,** 1812–1821, doi:10.1007/s11430-011-4333-8.

Dai, A., K. E. Trenberth, and T. R. Karl, 1998: Global variations in droughts and wet spells: 1900–1995. *Geophys. Res. Lett.,* **25,** 3367–3370, doi:10.1029/98GL52511.

Deryng, D., W. J. Sacks, C. C. Barford, and N. Ramankutty, 2011: Simulating the effects of climate and agricultural management practices on global crop yield. *Global Biogeochem. Cycles,* **25,** GB2006, doi:10.1029/2009GB003765.

Dinar, S., and A. Dinar, 2003: Recent developments in the literature on conflict negotiation and cooperation over shared international fresh waters. *Nat. Resour. J.,* **43,** 1217–1286.

Folland, C. K., and Coauthors, 2001a: Global temperature change and its uncertainties since 1861. *Geophys. Res. Lett.,* **28,** 2621–2624, doi:10.1029/2001GL012877.

——, and Coauthors, 2001b: Observed climate variability and change. *Climate Change 2001: The Scientific Basis,* J. T. Houghton et al., Eds., Cambridge University Press, 85–97.

Fyfe, J. C., N. P. Gillett, and G. J. Marshall, 2012: Human influence on extratropical Southern Hemisphere summer precipitation. *Geophys. Res. Lett.,* **39,** L23711, doi:10.1029/2012GL054199.

Gessner, U., V. Naeimi, I. Klein, C. Kuenzer, D. Klein, and S. Dech, 2013: The relationship between precipitation anomalies and satellite-derived vegetation activity in central Asia. *Global Planet. Change,* **110,** 74–87, doi:10.1016/j.gloplacha.2012.09.007.

Giorgi, F., 2006: Climate change hot-spots. *Geophys. Res. Lett.,* **33,** L08707, doi:10.1029/2006GL025734.

——, and R. Francisco, 2000: Evaluating uncertainties in the prediction of regional climate change. *Geophys. Res. Lett.,* **27,** 1295–1298, doi:10.1029/1999GL011016.

Harris, I., P. D. Jones, T. J. Osborna, and D. H. Listera, 2014: Updated high-resolution grids of monthly climatic observations—The CRU TS3.10 dataset. *Int. J. Climatol.,* **34,** 623–642, doi:10.1002/joc.3711.

Houghton, J. T., Y. Ding, D. J. Griggs, M. Noguer, P. J. van der Linden, X. Dai, K. Maskell, and C. A. Johnson, Eds., 2001: *Climate Change* 2001*: The Scientific Basis*. Cambridge University Press, 881 pp.

Hsiang, S. M., K. C. Meng, and M. A. Cane, 2011: Civil conflicts are associated with the global climate. *Nature,* **476,** 438–441, doi:10.1038/nature10311.

Hsu, P. C., T. Li, J.-J. Luo, H. Murakami, A. Kitoh, and M. Zhao, 2012: Increase of global monsoon area and precipitation under global warming: A robust signal? *Geophys. Res. Lett.,* **39,** L06701, doi:10.1029/2012GL051037.

Huang, A., Y. Zhang, and J. Zhu, 2009: Effects of the physical ensemble technique on simulation of the summer precipitation over China. *Acta Meteor. Sin.,* **6,** 713–724.

——, Y. R. Rao, and W. Zhang, 2012: On recent trends in atmospheric and limnological variables in Lake Ontario. *J. Climate,* **25,** 5807–5816, doi:10.1175/JCLI-D-11-00495.1.

Huang, D.-Q., J. Zhu, Y.-C. Zhang, and A.-N. Huang, 2013: Uncertainties on the simulated summer precipitation over Eastern China from the CMIP5 models. *J. Geophys. Res. Atmos.,* **118,** 9035–9047, doi:10.1002/jgrd.50695.

Huang, J., X. Guan, and F. Ji, 2012: Enhanced cold-season warming in semi-arid regions. *Atmos. Chem. Phys.,* **12,** 5391–5398, doi:10.5194/acp-12-5391-2012.

Hulme, M., 1996: Recent climatic change in the world's drylands. *Geophys. Res. Lett.,* **23,** 61–64, doi:10.1029/95GL03586.

Huxman, T. E., and S. D. Smith, 2001: Photosynthesis in an invasive grass and native forb at elevated CO_2 during an El Niño year in the Mojave Desert. *Oecologia,* **128,** 193–201, doi:10.1007/s004420100658.

Jiang, D. B., and Z. P. Tian, 2013: East Asian monsoon change for the 21st century: Results of CMIP3 and CMIP5 models. *Chin. Sci. Bull.,* **58,** 1427–1435, doi:10.1007/s11434-012-5533-0.

Jone, P. D., T. J. Osborn, and K. R. Briffa, 2001: The evolution of climate over the last millennium. *Science,* **292,** doi:10.1126/science.1059126.

Kharin, V. V., F. W. Zwiers, X. Zhang, and M. Wehner, 2013: Changes in temperature and precipitation extremes in the CMIP5 ensemble. *Climatic Change,* **119,** 345–357, doi:10.1007/s10584-013-0705-8.

Knutti, R., and J. Sedláček, 2012: Robustness and uncertainties in the new CMIP5 climate model projections. *Nat. Climate Change,* **3,** 369–373, doi:10.1038/nclimate1716.

Kucharik, C. J., 2008: Contribution of planting date trends to increased maize yields in the central United States. *Agron. J.,* **100,** 328–336, doi:10.2134/agrojnl2007.0145.

Leith, C. E., 1973: The standard error of time-average estimates of climatic means. *J. Appl. Meteor.,* **12,** 1066–1069, doi:10.1175/1520-0450(1973)012<1066:TSEOTA>2.0.CO;2.

Lioubimtseva, E., and G. Henebry, 2009: Climate and environmental change in arid central Asia: Impacts, vulnerability, and adaptations. *J. Arid Environ.,* **73,** 963–977, doi:10.1016/j.jaridenv.2009.04.022.

——, B. Simon, H. Faure, L. Faure-Denard, and J. M. Adams, 1998: Impacts of climatic change on carbon storage in the Sahara–Gobi desert belt since the Late Glacial Maximum. *Global Planet. Change,* **16–17,** 95–105, doi:10.1016/S0921-8181(98)00015-0.

——, R. Cole, J. M. Adams, and G. Kapustin, 2005: Impacts of climate and land-cover changes in arid lands of central Asia. *J. Arid Environ.,* **62,** 285–308, doi:10.1016/j.jaridenv.2004.11.005.

Lobell, D. B., and G. P. Asner, 2003: Climate and management contributions to recent trends in US agricultural yields. *Science,* **299,** 1032, doi:10.1126/science.1077838.

——, and C. B. Field, 2007: Global scale climate–crop yield relationships and the impacts of recent warming. *Environ. Res. Lett.,* **2,** 014002, doi:10.1088/1748-9326/2/1/014002.

Ma, Z., and C. Fu, 2007: Global aridification in the second half of the 20th century and its relationship to large-scale climate background. *Sci. China,* **50D,** 776–788, doi:10.1007/s11430-007-0036-6.

Melillo, J. M., A. D. McGuire, D. W. Kicklighter, B. Moore, C. J. Vorosmarty, and A. L. Schloss, 1993: Global climatic change and terrestrial net primary production. *Nature,* **363,** 234–240, doi:10.1038/363234a0.

Mitchell, T. D., and P. D. Jones, 2005: An improved method of constructing a database of monthly climate observations and associated high-resolution grids. *Int. J. Climatol.,* **25,** 693–712, doi:10.1002/joc.1181.

Narama, C., A. Kääb, M. Duishonakunov, and K. Abdrakhmatov, 2009: Spatial variability of recent glacier area changes in the Tien Shan Mountains, central Asia, using Corona (~1970), Landsat (~2000), and ALOS (~2007) satellite data. *Global Planet. Change,* **71,** 42–54, doi:10.1016/j.gloplacha.2009.08.002.

Narisma, G. T., J. A. Foley, R. Licker, and N. Ramankutty, 2007: Abrupt changes in rainfall during the twentieth century. *Geophys. Res. Lett.,* **34,** L06710, doi:10.1029/2006GL028628.

North G., T. Bell, R. Cahalan, and F. Moeng, 1982: Sampling errors in the estimation of empirical orthogonal functions. *Mon. Wea. Rev.,* **110,** 699–706, doi:10.1175/1520-0493(1982)110<0699:SEITEO>2.0.CO;2.

Peters, G. P., and Coauthors, 2013: The challenge to keep global warming below 2°C. *Nat. Climate Change,* **3,** 4–6, doi:10.1038/nclimate1783.

Peterson, T. C., and M. J. Manton, 2008: Monitoring changes in climate extremes: A tale of international collaboration. *Bull. Amer. Meteor. Soc.,* **89,** 1266–1271, doi:10.1175/2008BAMS2501.1.

Seo, K.-H., and J. Ok, 2013: Assessing future changes in the East Asian summer monsoon using CMIP3 models: Results from the best model ensemble. *J. Climate,* **26,** 1807–1817, doi:10.1175/JCLI-D-12-00109.1.

Sheffield, J., and E. F. Wood, 2008: Projected changes in drought occurrence under future global warming from multi-model, multi-scenario, IPCC AR4 simulations. *Climate Dyn.,* **31,** 79–105, doi:10.1007/s00382-007-0340-z.

Siegfried, T., T. Bernauer, R. Guiennet, S. Sellars, A. W. Robertson, J. Mankin, P. Bauer-Gottwein, and A. Yakovlev, 2012: Will climate change exacerbate water stress in central Asia? *Climatic Change,* **112,** 881–899, doi:10.1007/s10584-011-0253-z.

Smith, S. D., and Coauthors, 2000: Elevated CO_2 increases productivity and invasive species success in an arid ecosystem. *Nature,* **408,** 79–82, doi:10.1038/35040544.

Solomon, S., D. Qin, M. Manning, Z. Chen, M. Marquis, K. B. Averyt, M. Ignore, and H. L. Miller, Eds., 2007: *Climate Change 2007: The Physical Science Basis.* Cambridge University Press, 996 pp.

Taylor, K. E., R. J. Stouffer, and G. A. Meehl, 2012: An overview of CMIP5 and the experiment design. *Bull. Amer. Meteor. Soc.,* **93,** 485–498, doi:10.1175/BAMS-D-11-00094.1.

Trenberth, K. E., A. Dai, R. M. Rasmussen, and D. B. Parsons, 2003: The changing character of precipitation. *Bull. Amer. Meteor. Soc.,* **84,** 1205–1217, doi:10.1175/BAMS-84-9-1205.

van Vuuren, D. P., and Coauthors, 2011: The representative concentration pathways: An overview. *Climatic Change,* **109,** 5–31, doi:10.1007/s10584-011-0148-z.

Viviroli, D., and Coauthors, 2011: Climate change and mountain water resources: Overview and recommendations for research, management and policy. *Hydrol. Earth Syst. Sci.,* **15,** 471–504, doi:10.5194/hess-15-471-2011.

von Wehrden, H., J. Hanspach, K. Ronnenberg, and K. Wesche, 2010: Inter-annual rainfall variability in central Asia—A contribution to the discussion on the importance of environmental stochasticity in drylands. *J. Arid Environ.,* **74,** 1212–1215, doi:10.1016/j.jaridenv.2010.03.011.

Walsh, J., V. Kattsov, D. Portis, and V. Meleshko, 1998: Arctic precipitation and evaporation: Model results and observational estimates. *J. Climate,* **11,** 72–87, doi:10.1175/1520-0442(1998)011<0072:APAEMR>2.0.CO;2.

Wei, K., and Q. Bao, 2012: Projections of the East Asian winter monsoon under the IPCC AR5 scenarios using a coupled model: IAP_FGOALS. *Adv. Atmos. Sci.,* **29,** 1200–1214, doi:10.1007/s00376-012-1226-5.

Whitford, W., 2002: *Ecology of Desert Systems*. Academic Press, 343 pp.

Wolf, A. T., S. B. Yoffe, and M. Giordano, 2003: International waters: Identifying basins at risk. *Water Policy,* **5,** 29–60.